UNIVERSITY OF CALIFORNIA
SANTA CRUZ

PRELIMINARY INVESTIGATION OF MODELS OF COUPLED CLOCKS AND COUPLED DRIVEN PENDULUMS

A thesis submitted in partial satisfaction
of the requirements for the degree of

MASTER OF ARTS

in

MATHEMATICS

by

Christopher A. LeBailly

June 2013

The Thesis of Christopher A. LeBailly
is approved:

Professor Richard Montgomery, Chair

Professor Debra Lewis

Professor Jie Qing

Tyrus Miller
Vice Provost and Dean of Graduate Studies

Table of Contents

List of Figures

Abstract

Preliminary Investigation of Models of Coupled Clocks and Coupled Driven Pendulums

by

Christopher A. LeBailly

In this paper we study a phenomena observed in the 17$^{\text{th}}$ century by Christiaan Huygens. He found that two pendulum clocks placed on a common support synchronized over time. We study a model of this type of coupling primarily using the fourth-order Runge-Kutta method. We look at time series to get a picture of what types of synchronization occur and then once we figure out how to classify synchronization we study how varying the damping in the system affects the synchronization. We next look at what happens when driven pendulums replace the clocks. We compare phase portraits and bifurcation diagrams of the uncoupled driven pendulum to the coupled driven pendulums to get a picture of how the dynamics and chaotic tendencies of the driven pendulum change with the coupling.

Acknowledgments

I would first and foremost like to thank my master's thesis advisor, Richard Montgomery. Richard provided great support through out this project while at the same time giving me the freedom to explore several topics which I found interesting. He also provided different perspectives from mine and helped me find practical ways to investigates the questions which interested me. Next I would like to thank Debra Lewis for her input on my project at various stages as well as serving on my reading committee to give me feedback on this paper. I would also like to thank Jie Qing for serving on my reading committee.

I would also like to recognize my fellow graduate students. I am very appreciative of their support during this project and during my time at UCSC. In particular I would like to thank Christopher Toni for his input through out this project, from simply listening to me while I showed him my work, to bouncing ideas off of him when I was stuck, as well as his editorial comments. I would also like to thank my parents, Robert and Susan LeBailly, for their support and also for their nontechnical perspectives and editorial comments.

Chapter 1

Introduction

The Dutch mathematician and physicist Christiaan Huygens, who is credited with inventing the pendulum clock in 1656, made the startling observation that two pendulum clocks on a common support would synchronize over time. He described this phenomena in a letter he wrote to his father in 1665, which is partially quoted below ([3], pgs. 153-154)

> While I was forced to stay in bed for a few days and made observations on my two clocks of the new workshop, I noticed a wonderful effect that nobody could have thought of before. The two clocks, while hanging [on the wall] side by side with a distance of one or two feet between, kept in pace relative to each other with a precision so high that the two pendulums always swung together, and never varied. While I admired this for some time, I finally found that this happened due to a sort of sympathy: when I made the pendulums swing at differing paces, I found that half an hour later, they always returned to synchronism and kept it constantly afterwards, as long as I let them go.

As a high school student I was interested in computer modeling. My physics teacher told me about Huygens' discovery and thought it would be interesting to try to model this phenomena. I was also curious what would happen if the clocks were replaced by double pendulums since they exhibit chaotic behavior. I attempted to model the connecting beam as several point masses connected by springs. When I attempted this simulation it did not work. The position of the point masses grew larger and larger until the simulation ran out of memory. As far as I could discern my coding was correct and the problem came from the model and/or the numerical method. After unsuccessfully trying to fix it, I left this problem. In this paper I return to the same questions that intrigued me as a high schooler, however with a revised model and a few other tools on my belt.

Chapter 2

Modeling Techniques

2.1 Lagrangian Mechanics

In Newtonian mechanics we consider the forces acting on the system to find the equations of motion. However for more complicated systems this can become quite tedious. It is easier to compute the kinetic and potential energy for the conservative forces since these are scalar quantities (and forces are vectors). Using these energies we can use the Lagrangian approach to derive the equations of motion.

Let T represent the kinetic energy of a system and let V represent the potential energy. The Lagrangian is defined as $L := T - V$. Lagrange's equations states that

$$\frac{d}{dt}\left(\frac{\partial L}{\partial \dot{q_j}}\right) = \frac{\partial L}{\partial q_j} \tag{2.1}$$

where $\{q_j\}_{j=1}^n$ are the generalized coordinates and $\{\dot{q_j}\}_{j=1}^n$ are the generalized velocities of the system. If the system has non-conservative forces Q_j (such as friction) which affect the j^{th} generalized coordinate we can incorporate them into Lagrange's equation as follows:

$$\frac{d}{dt}\left(\frac{\partial L}{\partial \dot{q_j}}\right) - \frac{\partial L}{\partial q_j} = Q_j. \tag{2.2}$$

More information about Lagrangian mechanics, such as the derivation of Equations 2.1 and 2.2, can be found in several sources (such as [1]).

2.2 Krasovskii-Lasalle Invariance Principle

We will now develop some machinery to determine the stability of some of the systems we will study. We follow the definitions and theorems given in [2]. A continuous function $V(x)$ is *positive definite* if $V(x) > 0$ for all $x \neq 0$ and $V(0) = 0$. Similarly, a function is *negative definite* if $V(x) < 0$ for all $x \neq 0$ and $V(0) = 0$. We say that a function $V(x)$ is *positive semidefinite* if $V(x)$ can be zero at points other than $x = 0$ but otherwise $V(x)$ is strictly positive. We say $V(x)$ is *negative semidefinite* if $V(x)$ can be zero at points other than $x = 0$ but otherwise $V(x)$ is strictly negative.

Suppose we have a time-invariant system $\dot{x} = F(x)$, where $x \in \mathbb{R}^n$ and $\dot{x}$ denotes the time derivative of x. Let $x(t; x_0, t_0)$ denote the solution of this equation at time t with the initial condition $x(t_0) = x_0$. The set $M \subset \mathbb{R}^n$ is said to be an *invariant set* if for all $y \in M$ and $t_0 \geq 0$, we have $x(t; y, t_0) \in M$ for all $t \geq t_0$.

We want to know what happens as $t \to \infty$. We say x_e is (locally) *asymptotically stable* if for all $\epsilon > 0$, there exists a $\delta > 0$ such that

$$\|x(0) - x_e\| < \delta \Rightarrow \|x(t) - x_e\| < \epsilon \text{ for all } t > 0$$

and $x(t) \to x_e$ as $t \to \infty$ for $x(t)$ sufficiently close to x_e. Heuristically this mean that all nearby points converge to the equilibrium point.

Theorem 2.1. (Krasovskii-LaSalle Principle). Let $V : \mathbb{R}^n \to \mathbb{R}$ be a locally positive definite function such that on the compact set $\Omega_r = \{x \in \mathbb{R}^n : V(x) \leq r\}$ we have $\dot{V}$ is negative semidefinite. Define $S = \{x \in \Omega_r : \dot{V}(x) = 0\}$. As $t \to \infty$, the trajectory tends to the largest invariant subset of S. In particular, if S contains no nontrivial invariant sets then 0 is asymptotically stable. The function V is an “energy-like” function called a *Lyapunov function*.

2.3 Runge-Kutta Method

Most Calculus students learn Euler’s method to numerically solve differential equations. The formula simply states that for a differential equation $\dot{y} = f(t, y)$,

$$y_{n+1} = y_n + hf(t_n, y_n) \text{ and } t_{n+1} = t_n + h$$

where h is the step size. While this is a useful method for educational purposes, it is not very useful in practice. This method is not as accurate as other methods using the same step size nor is it as stable as others.

For this paper we will use a fourth-order Runge-Kutta method. This method states that for the differential equation $\dot{y} = f(t, y)$,

$$
\begin{aligned}
k_1 &= hf(t_n, y_n) \\
k_2 &= hf\left(t_n + \frac{h}{2}, y_n + \frac{k_1}{2}\right) \\
k_3 &= hf\left(t_n + \frac{h}{2}, y_n + \frac{k_2}{2}\right) \\
k_4 &= hf\left(t_n + h, y_n + k_3\right) \\
y_{n+1} &= y_n + \frac{k_1}{6} + \frac{k_2}{3} + \frac{k_3}{3} + \frac{k_4}{4} \\
t_{n+1} &= t_n + h
\end{aligned}
$$

where h is the step size.

In this paper we will study many second order differential equations. To numerically solve them we will rewrite them into a system of first order equations. Suppose that $\ddot{y} = g(t, y, \dot{y})$. If $v = \dot{y}$, then $\dot{v} = \ddot{y} = g(t, y, \dot{y})$. This gives rise to the system

$$
\begin{cases}
\dot{y} & = v \\
\dot{v} & = g(t, y, \dot{y}).
\end{cases}
$$

We can then apply the Runge-Kutta method to this system of equations to numerically solve the differential equation.

Chapter 3

Relevant Dynamical Systems

Next we will study some simple dynamical systems which will be important in the work to follow. A reader with some physics background will probably have seen these systems before and the derivation of the equations of motion using Newtonian mechanics. Here we shall derive these equations using Lagrangian mechanics outlined above to help the reader grasp the use of the Lagrangian method.

3.1 Springs: Simple Harmonic Oscillators

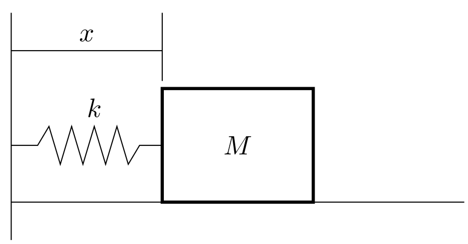

Figure 3.1: A Spring on a Frictionless Surface

We will first examine ideal springs. Hooke's law tells us that $F = -kx$ where x is the displacement from the spring's rest length and k is the spring constant. Since $F = ma = m\ddot{x}$ we find that $\ddot{x} = -\frac{k}{m}x$. We can also arrive at this using Lagrangian mechanics. The kinetic energy of the mass at the end of the spring is $\frac{1}{2}m\dot{x}^2$ and the potential energy stored in the spring is $\frac{1}{2}kx^2$. Hence we find that $L = \frac{1}{2}m\dot{x}^2 - \frac{1}{2}kx^2$. Applying Lagrange's Equation 2.1, we find that

$$m\ddot{x} = -kx. \tag{3.1}$$

To visualize solutions to these systems we plot the position x horizontal and the velocity $\dot{x}$ vertically. Such a plot is called a *phase portrait*. Numerically integrating Equation 3.1, using the Runge-Kutta method outlined in Section 2.3 and the Python programing language, with $k = m$ we get the phase portrait shown in Figure 3.2a.

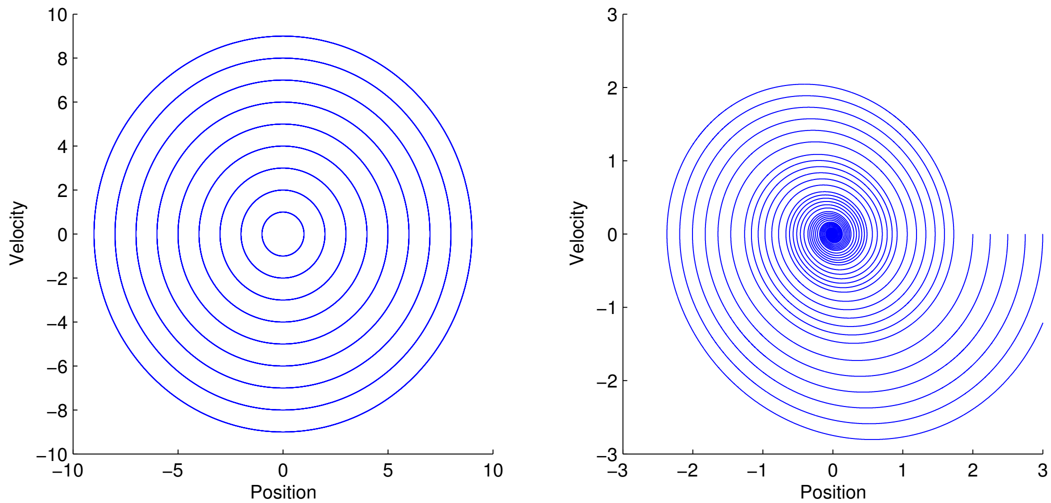

(a) Undamped Spring

(b) Damped Spring

Figure 3.2: Phase Portraits for Damped and Undamped Springs

A more realistic model accounts for friction. Applying Lagrange's Equation 2.2 with $Q_x = -\mu\dot{x}$ we find that

$$m\ddot{x} + \mu\dot{x} + kx = 0. \tag{3.2}$$

Numerically integrating Equation 3.2 with $k = m$ and $\mu/m = 0.2$ we get the phase portrait shown in Figure 3.2b.

It is clear from the phase portraits that over time all of the trajectories will tend to the origin. We can prove this using Krasovskii-LaSalle principle. To do this, consider the function

$$V = \frac{1}{2}m\dot{x}^2 + \frac{1}{2}kx^2. \tag{3.3}$$

Taking a derivative of V and substituting in Equation 3.2, we find $\dot{V} = m\dot{x}\ddot{x} + kx\dot{x} = m\dot{x}\ddot{x} - \dot{x}(m\ddot{x} + \mu\dot{x}) = -\mu\dot{x}^2$. Hence V is positive definite and $\dot{V}$ is negative semidefinite. Consider the set $S = \{(x, \dot{x}) \in \mathbb{R}^2 : \dot{V} = 0\}$. The Krasovskii-LaSalle principle tells us that any trajectory near the origin will tend towards the largest invariant subset of S. Since $\dot{V} = 0$ implies that $\dot{x} = 0$ we know $S = \{(x, \dot{x}) \in \mathbb{R}^2 : \dot{x} = 0\}$. For any trajectory contained in S we must have $\dot{x} = 0$ identically, meaning that $\ddot{x} = 0$. Hence by Equation 3.2, we find that $x = 0$. Accordingly the only trajectory in S is trivial, meaning the largest invariant subset of S is trivial. Ergo all trajectories are asymptotically stable to the origin.

3.2 Pendulums

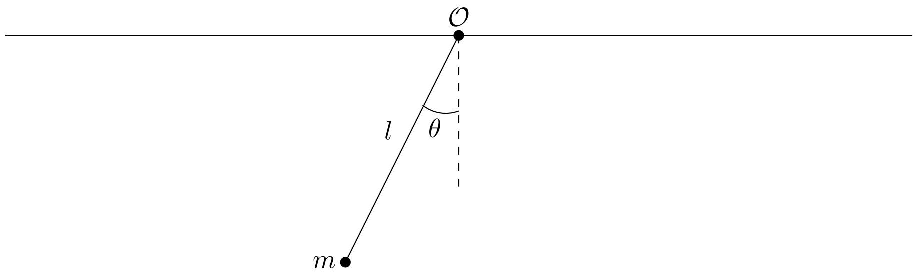

Figure 3.3: A Pendulum

Consider a point with mass m attached to a massless rod of length l (see Figure 3.3). If x represents the x-coordinate of the mass relative to $\mathcal{O}$ and y represents the y-coordinate of the mass relative to $\mathcal{O}$, then $x = l\sin\theta$ and $y = -l\cos\theta$. Hence

$$T = \frac{1}{2}m\big[\dot{x}^2 + \dot{y}^2\big] = \frac{1}{2}m\big[(l\dot{\theta}\cos\theta)^2 + (l\dot{\theta}\sin\theta)^2\big] = \frac{1}{2}ml^2\dot{\theta}^2.$$

The potential energy is simply $V = mgy = -mgl\cos\theta$, meaning $L = T - V = \frac{1}{2}ml^2\dot{\theta}^2 + mgl\cos\theta$. Applying Lagrange's Equation 2.1, we find

$$\ddot{\theta} + \frac{g}{l}\sin\theta = 0. \tag{3.4}$$

Numerically integrating Equation 3.4 with $g = l$ we find the phase portrait in Figure 3.4a.

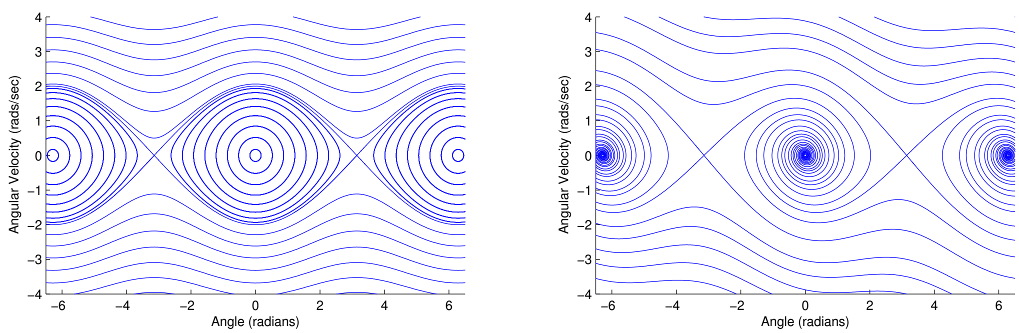

(a) Undamped Pendulum

(b) Damped Pendulum

Figure 3.4: Phase Portraits for Damped and Undamped Pendulums

Suppose that the pendulum experiences a frictional force of $Q_\theta = -\mu\dot{\theta}$. Applying Lagrange's Equation 2.2 we find

$$ml^2\ddot{\theta} + \mu\dot{\theta} + mgl\sin\theta = 0. \tag{3.5}$$

Numerically integrating Equation 3.5 with $g = l$ and $\mu/ml^2 = 0.2$ we get the phase portrait in Figure 3.4b.

We can again see that the damped pendulum has asymptotically stable equilibrium points. To show that the origin is asymptotically stable, consider the function

$$V = \frac{1}{2}ml^2\dot{\theta}^2 + mgl(1 - \cos\theta)$$

where $\theta \in (-\pi, \pi)$ ($\theta = \pm\pi$ gives unstable equilibria). Computing the the derivative and using Equation 3.5, we find $\dot{V} = ml^2\dot{\theta}\ddot{\theta} + mgl\sin(\theta)\dot{\theta} = -\dot{\theta}[gml\sin(\theta) + \mu\dot{\theta}] + mgl\sin(\theta)\dot{\theta} = -\mu\dot{\theta}^2$. Hence V is locally positive definite and $\dot{V}$ is negative semidefinite. Now consider $S = \{(\theta, \dot{\theta}) \in \mathbb{R}^2 : \dot{V} = 0\}$. We want to find the largest invariant subset of S. Since $\dot{V} = 0$ implies that $\dot{\theta} = 0$, we know any trajectory must have $\dot{\theta} = 0$ identically. This means that $\ddot{\theta} = 0$. Plugging this into Equation 3.5, we find that $\sin\theta = 0$. Since $\theta \in (-\pi, \pi)$, we see that $\theta = 0$. Hence the only trajectory in S is where $(\theta, \dot{\theta}) = (0, 0)$, which by the Krasovskii-LaSalle principle shows that the origin is asymptotically stable.

3.3 Clocks

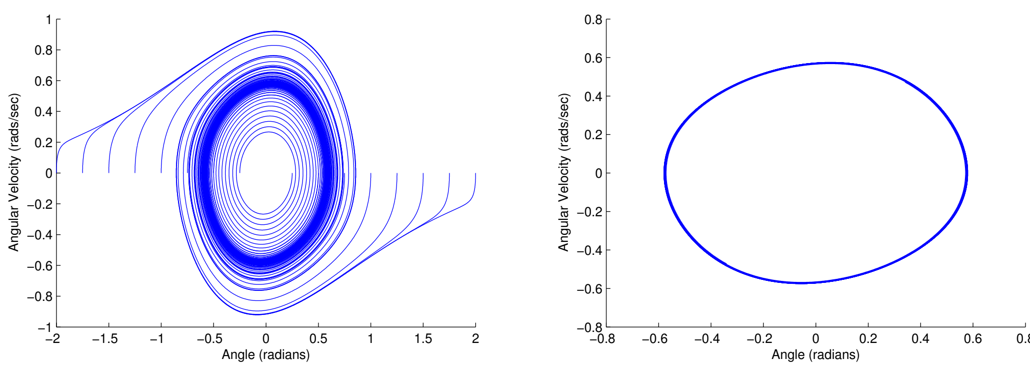

(a) Phase Portrait for Clock

(b) Limit Cycle for Clock

Figure 3.5: Phase Portraits and Limit Cycle of Clocks

Clocks clearly encounter fiction. A mechanism called an escapement supplies energy so clocks keep ticking. Following the model outlined in [5], we model the escapement as a Van der Pol oscillator. The escapement adds an external torque $D(\theta, \dot{\theta}) = e(\gamma^2 - \theta^2)\dot{\theta}$ where e is a constant which represents the strength of the escapement and γ represents the critical angle. If $|\theta| < \gamma$ then the escapement will supply energy to the pendulum. If $|\theta| > \gamma$ the escapement will dampen the pendulum. Adding the escapement makes $Q_\theta = -\mu\dot{\theta} + e(\gamma^2 - \theta^2)\dot{\theta}$, which yields

$$\ddot{\theta} = -\frac{g}{l}\sin\theta - \frac{\mu}{ml^2}\dot{\theta} + \frac{e}{ml^2}(\gamma^2 - \theta^2)\dot{\theta}. \tag{3.6}$$

Numerically integrating Equation 3.6 for four minutes we get the phase portrait in Figure 3.5a. If we only plot the last two minutes of the simulation we can easily see that all initial conditions tend to the same limit cycle, shown in Figure 3.5b. For both simulations $g = l$, $\mu/ml^2 = 0.2$, $e/ml^2 = 1.2$, and $\gamma = 0.5$.

3.4 Driven Pendulum

The driven pendulum is similar to a normal pendulum, except that the driven pendulum is driven by an external force of $A\cos(\omega t)$, where A is the forcing amplitude and ω is related to the forcing frequency. Unlike the escapement in a clock, this forcing is a function of time. While it is periodic, it may or may not coincide with the natural frequency of the pendulum. This can result in periodic, quasi-periodic, or chaotic behavior.

The Lagrangian for the driven pendulum is the same as the pendulum. Since there is a nonconservative driving forcing of $A\cos(\omega t)$ and a damping of $-\mu\dot{\theta}$, we have $Q_\theta = A\cos(\omega t) - \mu\dot{\theta}$. Using Equation 2.2 we find

$$ml^2\ddot{\theta} + mgl\sin\theta + \mu\dot{\theta} = A\cos(\omega t). \tag{3.7}$$

A phase portrait for the driven pendulum is plotted in Figure 3.6a with $ml^2 = mgl = 1$, $\mu = 1/4$, $A = 3/2$, and $\omega = 2/3$. These conditions result in chaotic behavior which gives rise to a cluttered phase portrait.

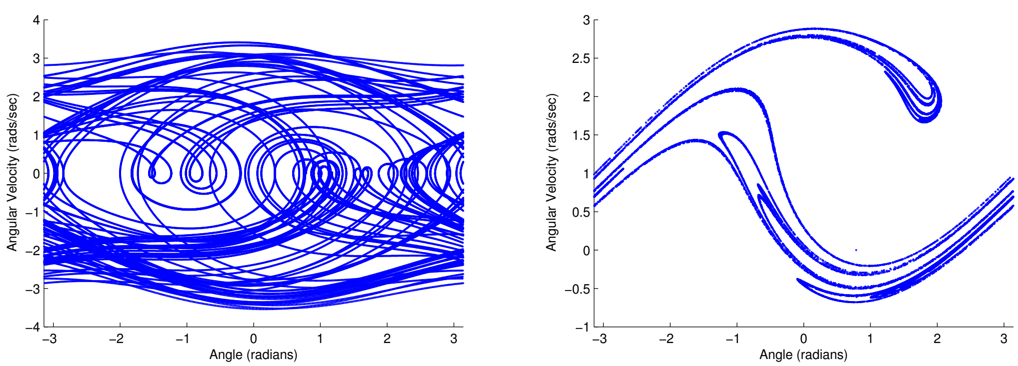

(a) Phase Portrait for Driven Pendulum

(b) Poincaré Section for Driven Pendulum

Figure 3.6: Phase Portrait and Poincaré Section for the Driven Pendulum

One way to see more interesting features of the driven pendulum is to create a Poincaré section. Imagine that we place the driven pendulum in a dark room, but turn a light on at a fixed frequency to record the pendulum's angle and angular velocity. We can then use this data to create a phase portrait. If we strobe the pendulum at the same frequency as the driving force, we get the Poincaré section shown in Figure 3.6b.

Another way to study the driven pendulum is through bifurcation diagrams. Suppose we fix all the parameters except for one. We still strobe the pendulum but just record the angular velocity. We then plot the angular velocity vertically and the parameter we vary horizontally. We can vary the forcing amplitude (Figure 3.7), the drive frequency (Figure 3.8), and the damping (Figure 3.9). If we look at the damping bifurcation diagram, we have periodic motion when $\mu > 0.5$. We get quasi-periodic motion when $\mu \approx 0.42$. We get chaotic motion when $\mu < 0.1$.

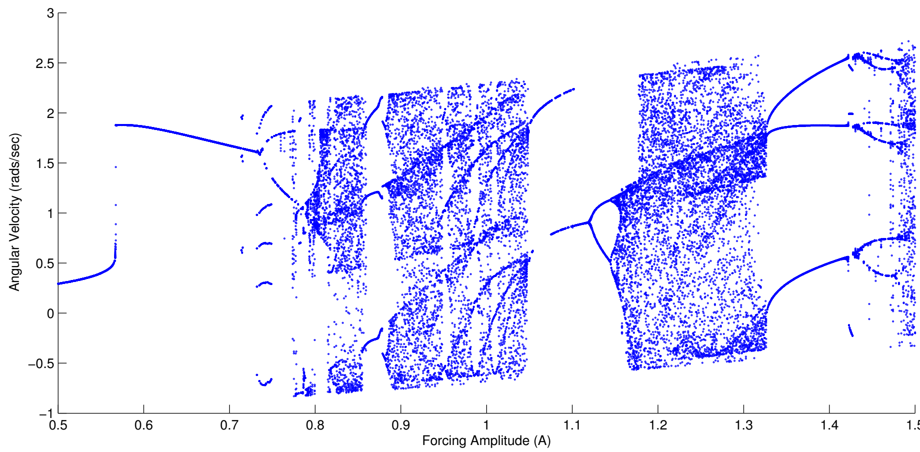

Figure 3.7: Forcing Bifurcation Diagram

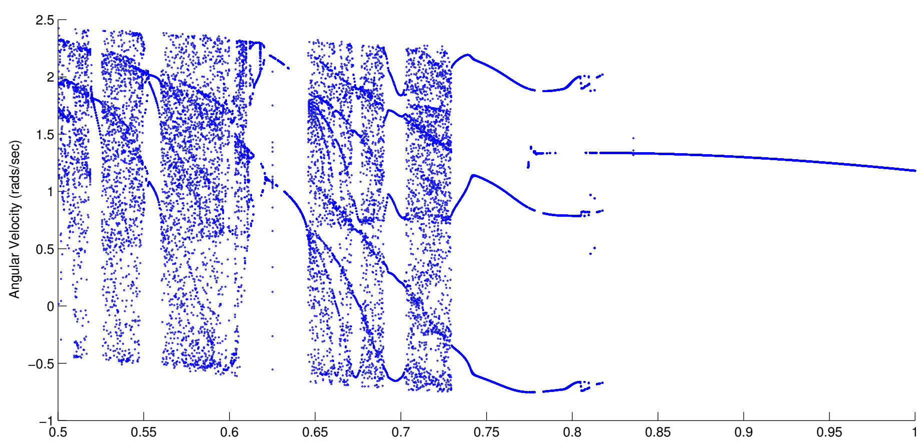

Figure 3.8: Drive Frequency Bifurcation Diagram

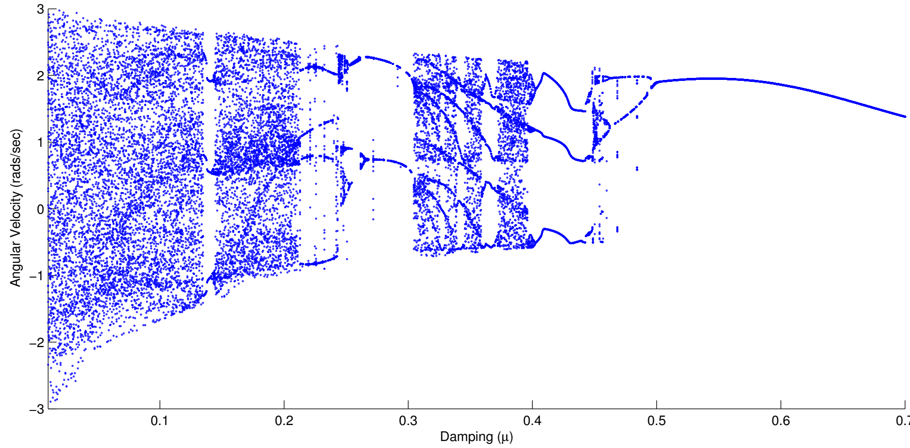

Figure 3.9: Damping Bifurcation Diagram

3.5 Error in Runge-Kutta Method

A simple way to gauge the error committed by the Runge-Kutta algorithm is to compare the predicted theoretical energy of the system to the energy of the of the simulated system. For this method to work we need the energy to be conserved. Hence this method will only work for the frictionless spring and the frictionless pendulum, as all the other systems have nonconservative forces. Recall that relative error is given by $|E_p - E_s|/E_p$, where E_p is the predicted theoretical energy and E_s is the simulated energy. In Figure 3.10a we show the relative error versus time for the spring with a step size of 0.01. In Figure 3.10b we show the relative error for the pendulum with a step size of 0.001.

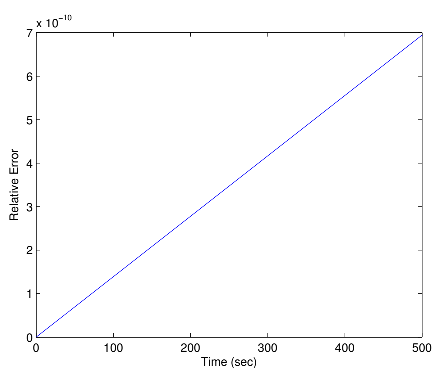

(a) Error for Spring

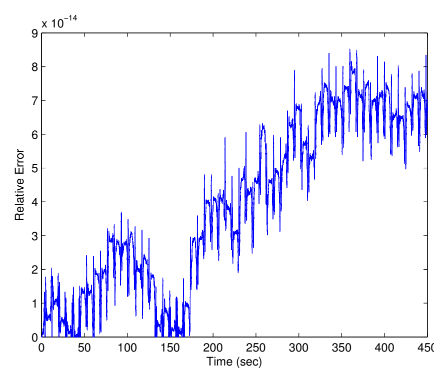

(b) Error for Pendulum

Figure 3.10: Error encountered using Runge-Kutta for our Conservative Systems

Chapter 4

A Model of Two Coupled Clocks

4.1 Experimental Results Motivating Our Model

In [4], the authors attempted to reproduce Huygens' result experimentally. They first mounted two pendulum clocks to a wall. However they did not observe synchronization. Next they took two tables and placed a block of wood which spanned the gap between the tables. They then hung the two pendulum clocks from the beam. However they still did not observe synchronization. Next they placed two small cylindrical rollers under the beam so the beam could move back and forth. This modification made both in-phase and out-of-phase synchronization possible. Since it was experimentally shown that this set-up causes the clocks to synchronize it will serve as the basis for our model.

4.2 Model and Equations of Motion

In this model we will consider two pendulums with length l and point mass m attached at the end, affixed to a common support of mass M (as shown in Figure 4.1). The common support is then attached to a spring of spring constant k. As the common support moves it experiences damping. Suppose that the pendulums have an escapement mechanism described by $D_i = e(\gamma^2 - \theta_i^2)\dot{\theta}_i$ which is the Van der Pol term we used to model clocks ($i = 1$ or 2). Let x measure the displacement of the support (with $x = 0$ corresponding to the spring at its rest length), and let α and β be fixed distances with $\beta > 2l$ (ensuring the pendulums never collide).

If x_l represents the x-coordinate of the left pendulum relative to $\mathcal{O}$ and y_l represents the y-coordinate of the left pendulum relative to $\mathcal{O}$, then $x_l = x + \alpha + l\sin\theta_1$ and $y_l = -l\cos\theta_1$. Hence the kinetic energy from the left pendulum is

$$T_l = \frac{1}{2}m(\dot{x_l}^2 + \dot{y_l}^2) = \frac{1}{2}m\big[(\dot{x} + l\dot{\theta}_1\cos\theta_1)^2 + (l\dot{\theta}_1\sin\theta_1)^2\big].$$

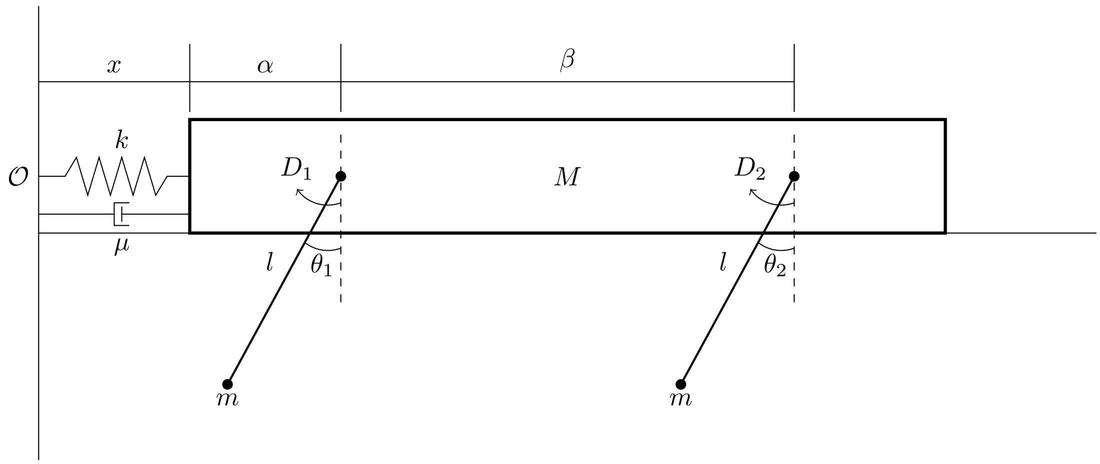

Figure 4.1: Two Pendulums on a Moving Support, Attached to a Damped Spring

Similarly if x_r represents the x-coordinate of the right pendulum relative to $\mathcal{O}$ and y_r represents the y-coordinate of the right pendulum relative to $\mathcal{O}$, then $x_l = x + \alpha + \beta + l\sin\theta_2$ and $y_l = -l\cos\theta_2$. Hence the kinetic energy from the right pendulum is

$$T_r = \frac{1}{2}m(\dot{x_r}^2 + \dot{y_r}^2) = \frac{1}{2}m\big[(\dot{x} + l\dot{\theta_2}\cos\theta_2)^2 + (l\dot{\theta_2}\sin\theta_2)^2\big].$$

Since the kinetic energy of the support is simply $\frac{1}{2}M\dot{x}^2$ we find the total kinetic energy is

$$T = \frac{1}{2}(M+2m)\dot{x}^2 + ml\dot{x}\big[\dot{\theta_1}\cos\theta_1 + \dot{\theta_2}\cos\theta_2\big] + \frac{1}{2}ml^2\big[\dot{\theta_1}^2 + \dot{\theta_2}^2\big].$$

The potential energy is simply the sum of the energy stored in the spring plus the gravitation potential of the two pendulums, which is

$$V = \frac{1}{2}kx^2 + mgy_l + mgy_r = \frac{1}{2}kx^2 - mgl\cos\theta_1 - mgl\cos\theta_2.$$

Hence we find the Lagrangian of the system is

$$L = \frac{1}{2}\big(M+2m\big)\dot{x}^2 + ml\dot{x}\big[\dot{\theta_1}\cos\theta_1 + \dot{\theta_2}\cos\theta_2\big] + \frac{1}{2}ml^2\big[\dot{\theta_1}^2 + \dot{\theta_2}^2\big] - \frac{1}{2}kx^2 + mgl\cos\theta_1 + mgl\cos\theta_2.$$

Since not all the forces are conservative, we must use Langrange's Equation 2.2. The friction in the frame is incorporated with $Q_x = -\mu\dot{x}$, the escapement for the left pendulum is incorporated with $Q_{\theta_1} = D_1 = e(\gamma^2 - \theta_1^2)\dot{\theta}_1$ and similarly the escapement for the right pendulum is incorporated with $Q_{\theta_2} = D_2 = e(\gamma^2 - \theta_2^2)\dot{\theta}_2$. Applying Lagrange's Equation 2.2 with the three generalized coordinates x, θ_1, θ_2 yields

$$\left\{\begin{array}{rcl} gml\sin\theta_1 + ml\ddot{x}\cos\theta_1 + ml^2\ddot{\theta}_1 & = & e(\gamma^2 - \theta_1^2)\dot{\theta}_1 \\ gml\sin\theta_2 + ml\ddot{x}\cos\theta_2 + ml^2\ddot{\theta}_2 & = & e(\gamma^2 - \theta_2^2)\dot{\theta}_2 \\ (M+2m)\ddot{x} + kx + \mu\dot{x} + ml\big[\ddot{\theta}_1\cos\theta_1 + \ddot{\theta}_2\cos\theta_2\big] & = & ml\big[\dot{\theta_1}^2\sin\theta_1 + \dot{\theta_2}^2\sin\theta_2\big]. \end{array}\right. \qquad (4.1)$$

4.3 Asymptotic Stability with Krasovskii-LaSalle

Following the ideas in [5] we can show a simplified version of Equation 4.1 tends to out-of-phase synchronization. When we use the Krasovskii-LaSalle principle, we want to define our coordinates such that the origin is the asymptotically stable point. Since we are interested in showing that trajectories tend towards out-of-phase synchronization, we want to introduce the variable $\theta = \theta_1 + \theta_2$. Doing so means out-of-phase synchronization will be achieved when $\theta = \dot{\theta} = 0$. However we can not introduce this in Equation 4.1. We can simplify Equation 4.1 by linearizing the trigonometric functions and dropping the squared terms. After doing this we can add the first two equations in 4.1 to get θ. Doing so yields

$$\begin{cases} gml\theta + 2ml\ddot{x} + ml^2\ddot{\theta} = 0 & \text{(4.2a)} \\ (M+2m)\ddot{x} + kx + \mu\dot{x} + ml\ddot{\theta} = 0. & \text{(4.2b)} \end{cases}$$

Consider the function

$$V = mgl\theta^2 + 2klx^2 + 2M\dot{x}^2 + m(l\dot{\theta} + 2\dot{x})^2. \tag{4.3}$$

It is clear that V is positive definite. Differentiating V and using Equation 4.2, we find

$$\begin{aligned} \dot{V} &= 2mgl\theta\dot{\theta} + 2ml^2\dot{\theta}\ddot{\theta} + 4kx\dot{x} + 4M\dot{x}\ddot{x} + 8m\dot{x}\ddot{x} + 4ml[\ddot{\theta}\dot{x} + \dot{\theta}\ddot{x}] \\ &= 2\dot{\theta}(mgl\theta + ml^2\ddot{\theta}) + 4kx\dot{x} + 4(M+2m)\dot{x}\ddot{x} + 4ml[\ddot{\theta}\dot{x} + \dot{\theta}\ddot{x}] \\ &= 2\dot{\theta}(mgl\theta + ml^2\ddot{\theta}) + 4\dot{x}[kx + (M+2m)\ddot{x}] + 4ml\ddot{\theta}\dot{x} + 4ml\dot{\theta}\ddot{x} \\ &= 2\dot{\theta}(-2ml\ddot{x}) + 4\dot{x}[-\mu\dot{x} - ml\ddot{\theta}] + 4ml\ddot{\theta}\dot{x} + 4ml\dot{\theta}\ddot{x} \\ &= -4ml\dot{\theta}\ddot{x} - 4\mu\dot{x}^2 - 4ml\dot{x}\ddot{\theta} + 4ml\ddot{\theta}\dot{x} + 4ml\dot{\theta}\ddot{x} \\ &= -4\mu\dot{x}^2. \end{aligned}$$

Hence $\dot{V}$ is negative semidefinite.

Let $S = \{(\theta, \dot{\theta}, x, \dot{x}) \in \mathbb{R}^4 : \dot{V} = 0\}$. The Krasovskii-LaSalle Principle tells us that any trajectory tends to the largest invariant subset of S. Since $\dot{V} = -4\mu\dot{x}^2$, $\dot{V} = 0$ implies that $\dot{x} = 0$. Since we are only interested in trajectories which are contained entirely within S, we know $\dot{x}$ must be identically zero which means that $\ddot{x} = 0$ and x is a constant. Applying this to Equation 4.2b we see that $kx + ml\ddot{\theta} = 0$ which means

$$\ddot{\theta} = -\frac{kx}{ml} = \text{constant}.$$

Applying this to Equation 4.2a we find that $gml\theta - lkx = 0$ which means that

$$\theta = \frac{kx}{gm} = \text{constant}.$$

This means that $\dot{\theta} = \ddot{\theta} = 0$. Since $\ddot{\theta} = \ddot{x} = 0$, Equation 4.2a tells us that $\theta = 0$. Hence the only invariant subset of S is $(\theta, \dot{\theta}, x, \dot{x}) = (0,0,0,0)$. Since the only invariant subset of S is trivial, the

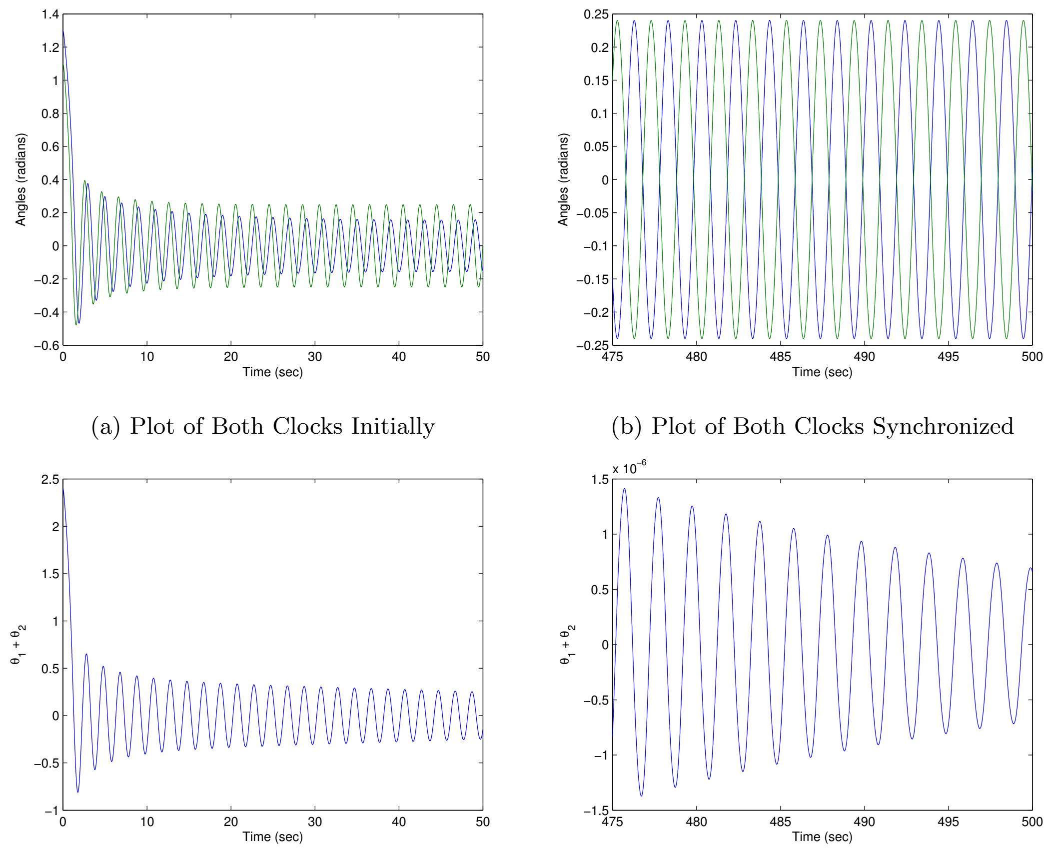

(a) Plot of Both Clocks Initially

(b) Plot of Both Clocks Synchronized

(c) Sum of Angles Initially

(d) Sum of Angles when Synchronized

Figure 4.2: Time Series for Out-of-Phase Synchronization

Krasovskii-LaSalle Principle tells us that the origin is asymptotically stable. Since $\theta = \theta_1 + \theta_2$, this shows that for all trajectories $\theta_1 + \theta_2$ tends to zero.

4.4 Investigation of Simulation

While the stability shown in Section 4.3 is interesting in that it shows the result Huygen's observed, it does not paint a complete picture. To fully understand what happens we need to return to Equation 4.1. We now will turn our attention to the numerical simulations using the Runge-Kutta method outlined in Section 2.3 and the Python programing language.

For our first simulation let $M = 5, k = 0.1, \mu = 7, m = 0.1, l = 1, e = 1.13, \gamma = 0.12$ and $g = 9.8$. We start with $\theta_1 = 1.3$, $\theta_2 = 1.1$ and $\dot{\theta}_1 = \dot{\theta}_2 = x = \dot{x} = 0$. Looking at a graph of the time series in Figure 4.2b of each pendulum they seem to be close to an out-of-phase synchronization. If the pendulums are exactly out-of-phase then we would expect $\theta_1 + \theta_2 = 0$.

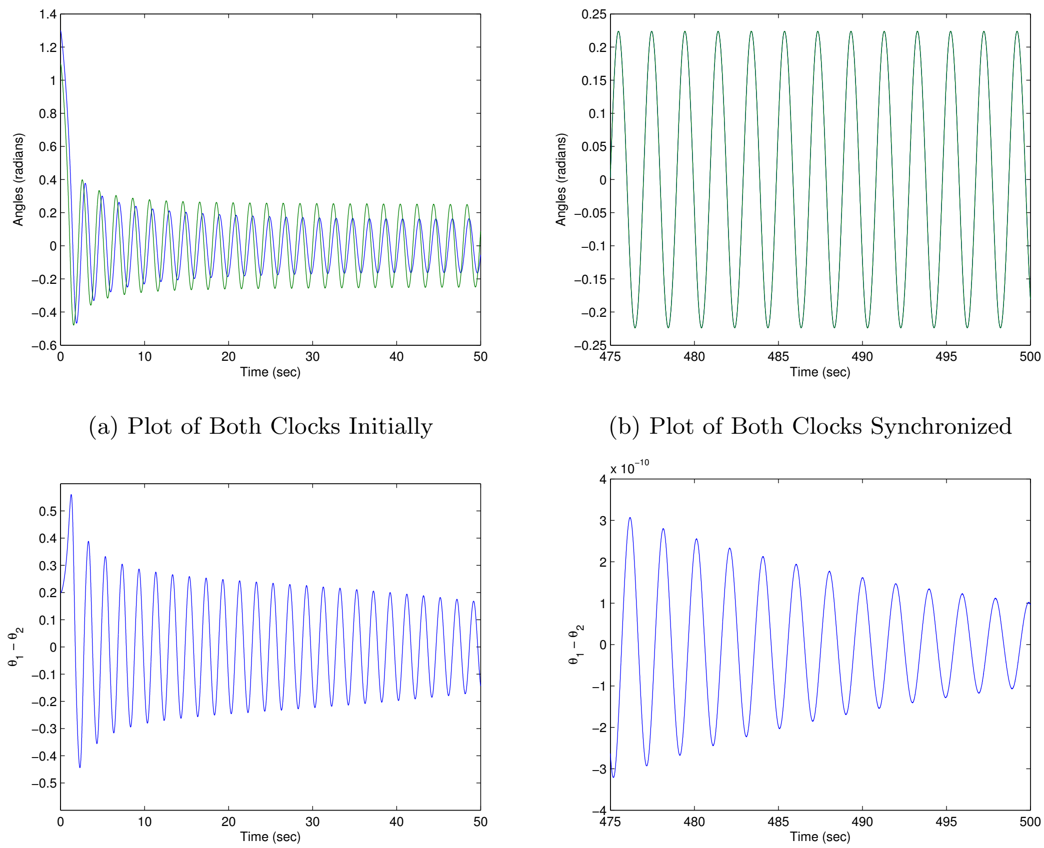

(a) Plot of Both Clocks Initially

(b) Plot of Both Clocks Synchronized

(c) Difference of Angles Initially

(d) Difference of Angles when Synchronized

Figure 4.3: Time Series for In-of-Phase Synchronization

Graphing $\theta_1+\theta_2$ versus time it appears that $\theta_1+\theta_2$ is tending towards zero, but is not identically zero, as shown in Figures 4.2c and 4.2d.

Now let's change the damping in the beam and let $\mu = 3$. Looking at a graph of the time series in Figure 4.3b of each pendulum they seem to be close to an in-phase synchronization. If the pendulums are in-phase then we would expect $\theta_1 - \theta_2 = 0$. Graphing $\theta_1 - \theta_2$ versus time it appears that $\theta_1 - \theta_2$ is tending towards zero, but is not identically zero, as shown in Figures 4.3c and 4.3d.

This raises the question of how do the dynamics change as we vary the damping in the beam. We have just seen for small damping that in-phase synchronization occurs and for larger damping out-of-phase synchronization occurs. What happens as we vary the damping? How does the system transition from in-phase to out-of-phase synchronization? To study this we need to develop a criteria for when synchronization is achieved.

The above time series graphs show that while either $\theta_1 + \theta_2$ or $\theta_1 - \theta_2$ is tending to zero, it does not become identically zero. Hence we define in-phase synchronization to mean there exists a T such that $|\theta_1(t) - \theta_2(t)| < \epsilon$ for all $t > T$ (where ϵ is small). We define out-of-phase synchronization to mean there exists a T such that $|\theta_1(t) + \theta_2(t)| < \epsilon$ for all $t > T$ (where ϵ is small). We will call T the time when synchronization is achieved. We can write a program to find the time when synchronization is achieved as we vary μ and to classify the type of synchronization, which is shown in Figure 4.4.

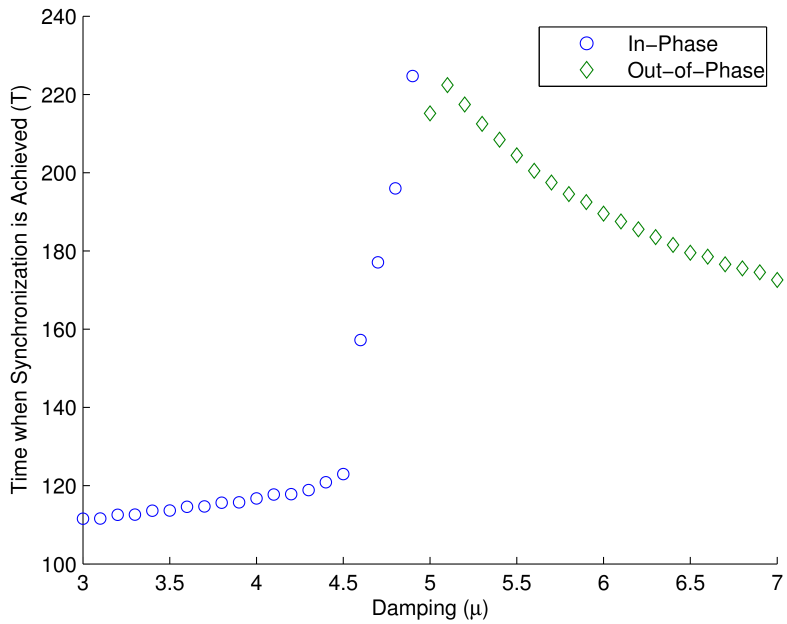

Figure 4.4: Time to Synchronize vs. Damping ($\epsilon = 0.01$)

This picture suggests there is a critical damping where the synchronization switches from in-phase to out-of-phase. We are interested in what happens at this critical damping. In order to study it we need to find where this critical damping occurs. Let μ_c be the critical damping. To estimate μ_c we will use a bisection method. We start with $\mu_{\text{min}} = 4$ which we know gives in-phase synchronization and $\mu_{\text{max}} = 6$ which gives out-of-phase synchronization. We test the midpoint to see what type of synchronization occurs. If in-phase synchronization occurs we replace μ_{min} with the midpoint. If out-of-phase synchronization is achieved, then μ_{max} is replaced with the midpoint. This is repeated until neither in-phase nor out-of-phase synchronization is detected at the midpoint. It is possible that synchronization occurs at a time greater than the time the simulation ran, but we know for sure that the actual critical damping must be between μ_{min} and μ_{max}. Running this we find that $4.96417299006 \leq \mu_c \leq 4.96417299029$. Figure 4.5 shows the time series where $\mu = 4.96417299018$ (the midpoint of the interval we found). As we can see, no synchronization occurs here.

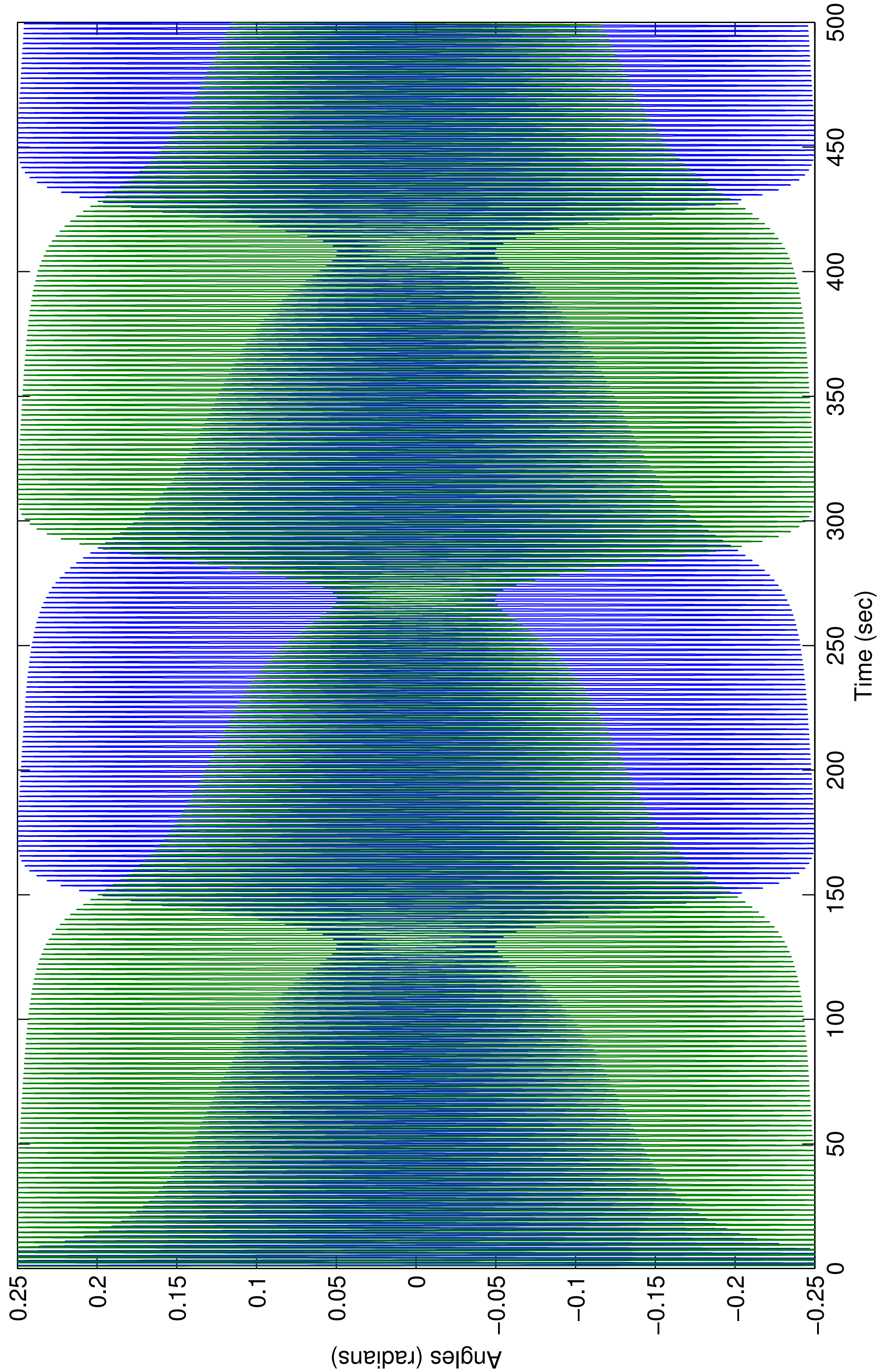

Figure 4.5: No Synchronization at Critical Damping

Chapter 5

Coupled Driven Pendulums

As a high schooler I was curious what would happen when two double pendulums were coupled in a fashion similar to Huygens' clocks. I was curious as to how the two chaotic oscillators would influence one another. I explained this to Richard Montgomery. He proposed that working with driven pendulums would be easier than double pendulums since there are fewer variables but still lets me look at the coupling of two chaotic oscillators. Another advantage to using two driven pendulums is that the equations of motion are very similar to the equations we used for the coupled clocks. We simply need to replace the equation of the clock escapement (which gives rise to a limit cycle as we saw in Section 3.3) with that of the time dependent function $A\cos(\omega t)$ (which can give rise to chaotic behavior as we saw in Section 3.4). While there is an abundance of work done looking at the coupling of chaotic oscillators, I did not find any papers which study this particular system.

5.1 Equations of Motion

The Lagrangian for this system is the same as the Lagrangian for the coupled clocks in the previous chapter. The only difference arises in the nonconservative forces. We simply need to replace the equation for the escapement with the equation for the time dependent driver. Hence $Q_{\theta_1} = Q_{\theta_2} = A\cos(\omega t)$. This yields the system

$$\left\{\begin{array}{rcl} gml\sin\theta_1 + ml\ddot{x}\cos\theta_1 + ml^2\ddot{\theta}_1 & = & A\cos(\omega t) \\ gml\sin\theta_2 + ml\ddot{x}\cos\theta_2 + ml^2\ddot{\theta}_2 & = & A\cos(\omega t) \\ (M+2m)\ddot{x} + kx + \mu\dot{x} + ml\big[\ddot{\theta}_1\cos\theta_1 + \ddot{\theta}_2\cos\theta_2\big] & = & ml\big[\dot{\theta}_1^{\,2}\sin\theta_1 + \dot{\theta}_2^{\,2}\sin\theta_2\big]. \end{array}\right. \tag{5.1}$$

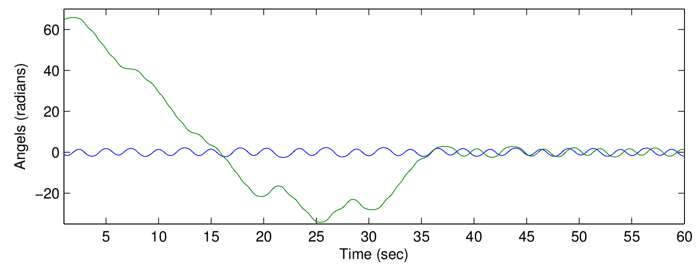

(a) Plot of Both Driven Pendulums (Part 1)

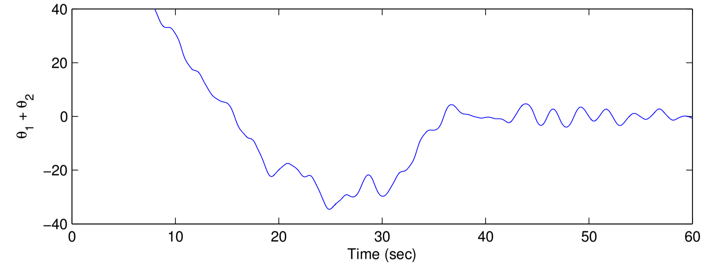

(b) Sum of Angles for Driven Pendulums (Part 1)

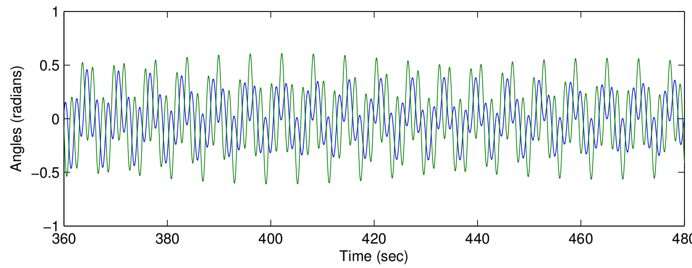

(c) Plot of Both Driven Pendulums (Part 2)

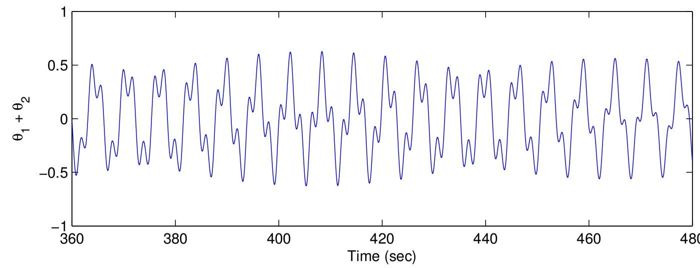

(d) Sum of Angles for Driven Pendulums (Part 2)

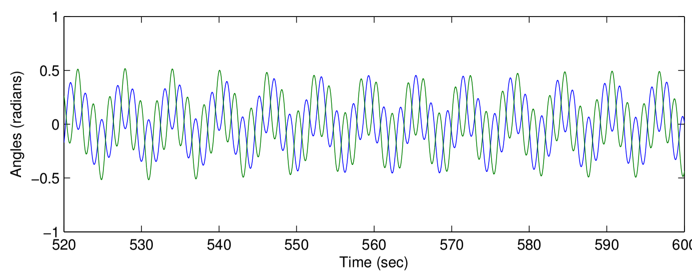

(e) Plot of Both Driven Pendulums (Part 3)

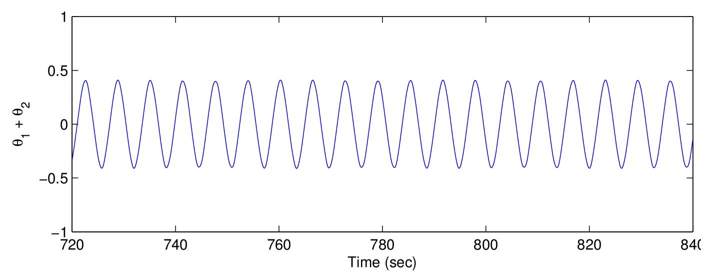

(f) Sum of Angles for Driven Pendulums (Part 3)

Figure 5.1: Time Series for Coupled Driven Pendulums

5.2 Time Series

Let's look at how this system evolves over time. For these simulations we let $M = 7.5$, $k = 0.11$, $\mu = 10$, $m = 0.1$, $l = 1.0$, $A = 0.17$, $\omega = 1$ and $g = 9.81$. We start at $\theta_1 = 2$, $\theta_2 = -2$, and $\dot{\theta}_1 = \dot{\theta}_2 = x = \dot{x} = 0$. As we can see, there is some irregular behavior at the start but it appears to settle down into nonchaotic behavior, as shown in Figure 5.1. Looking at the sum $\theta_1 + \theta_2$ also helps us see what is going on, which is displayed in Figures 5.1b, 5.1d, and 5.1f.

5.3 Phase Portraits

Let's now look at some phase portraits for the two coupled driven pendulums. We saw before in Section 3.4 that the phase portrait for the driven pendulum was very cluttered. However we see that when we look at the phase portraits for each of the driven pendulums, shown in Figure 5.2, they are much less cluttered.

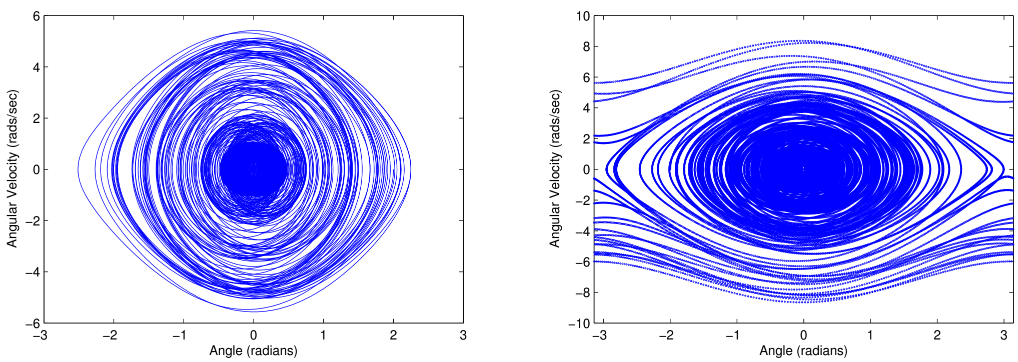

(a) Left Pendulum Phase Portrait

(b) Right Pendulum Phase Portrait

Figure 5.2: Phase Portraits for Coupled Driven Pendulums

Furthermore, if we only look at the second half of the data, it appears that the behavior is no longer chaotic, as shown in Figure 5.3. This suggests that over time the system becomes less chaotic. This is very surprising considering the behavior we observed for the uncoupled system. Of course this is for just one set of initial conditions and system parameters. Instead of looking at several phase portraits we can get the same information in a bifurcation diagram.

5.4 Bifurcation Diagrams

As we saw in Section 3.4, the bifurcation diagrams gave us an idea of when the system is periodic, quasi-periodic, or chaotic. The phase portraits we looked at in the previous section

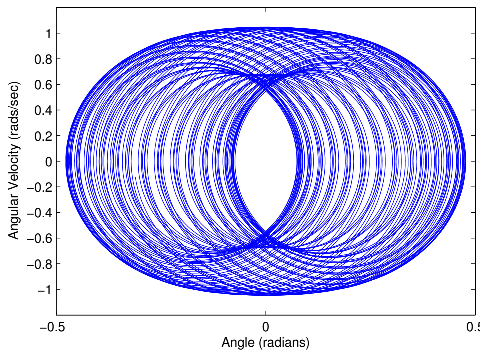

(a) Left Pendulum Limit Cycle

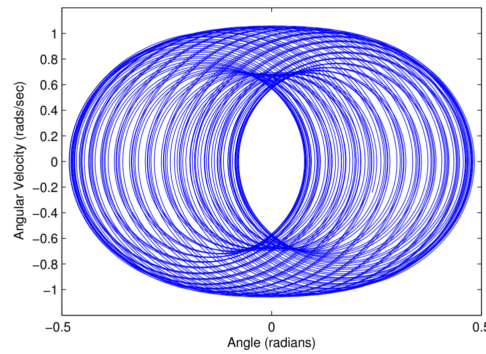

(b) Right Pendulum Limit Cycle

Figure 5.3: Limit Cycle for Coupled Driven Pendulums

suggest that the motion of both pendulums settles down. As we did in Section 3.4, we want to use the bifurcation diagram to see where we get periodic, quasi-periodic, or chaotic behavior.

Recall that we vary one of the parameters and record the angular velocity. We strobe the angular velocity at the same frequency as the driver. We only look at the second half of the data so we can see where the system tends to in the long run. The resulting bifurcation diagrams shows that we no longer get chaotic behavior for either driven pendulum as we vary forcing (Figure 5.4). If we vary the drive frequency (Figure 5.5) we also don't see chaotic behavior. Nevertheless we see some chaotic behavior for small damping (Figure 5.6). However when we compare the bifurcation diagrams for the coupled driven pendulums in Figures 5.4, 5.5, and 5.6 to the bifurcation diagrams of the uncoupled driven pendulums in Figures 3.7, 3.8, and 3.9 there are some striking differences. While the uncoupled system does have regions of periodic and quasi-periodic motion, much of the motion is dominated by chaos. However only a small portion of the bifurcation diagrams show chaos. This seems to suggest that the coupling reduces the chaotic tendencies of the driven pendulum.

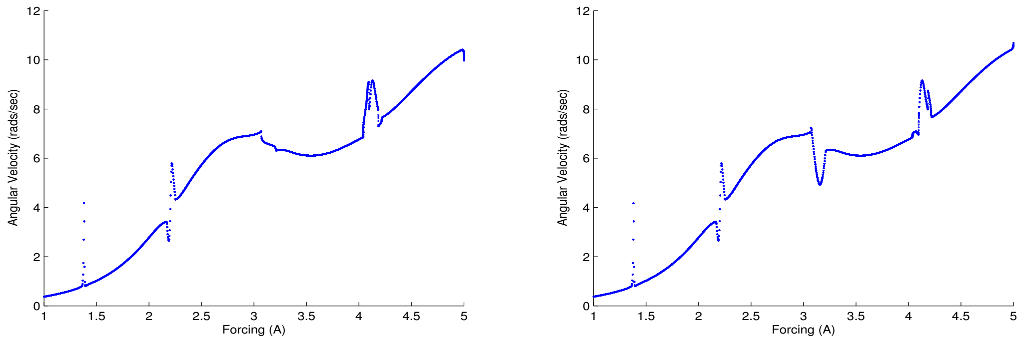

(a) Left Pendulum Bifurcation Diagram

(b) Right Pendulum Bifurcation Diagram

Figure 5.4: Forcing Bifurcation Diagrams

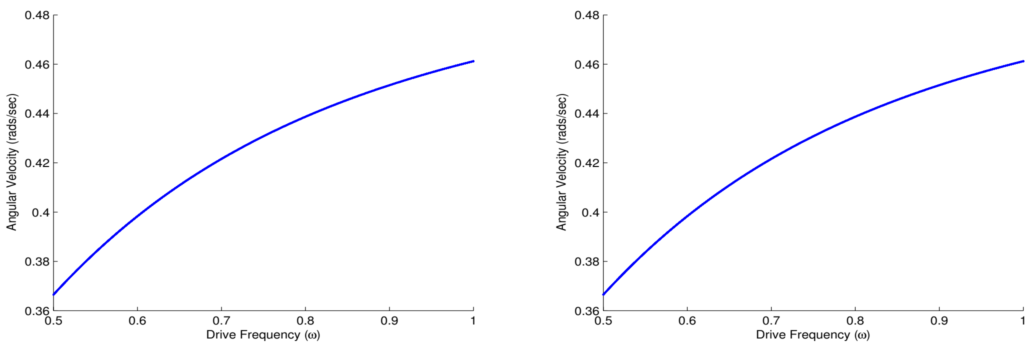

(a) Left Pendulum Bifurcation Diagram

(b) Right Pendulum Bifurcation Diagram

Figure 5.5: Drive Frequency Bifurcation Diagrams

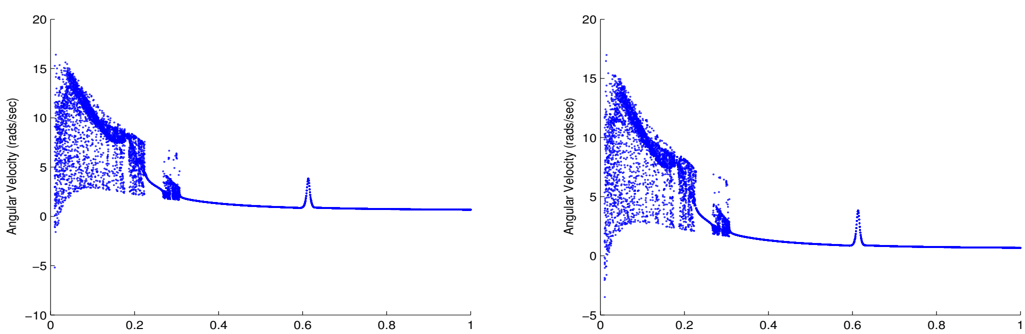

(a) Left Pendulum Bifurcation Diagram

(b) Right Pendulum Bifurcation Diagram

Figure 5.6: Damping Bifurcation Diagrams

Chapter 6

Future Work and Conclusions

The biggest surprise encountered in this work was with the coupled driven pendulums. Seeing this coupling of two chaotic oscillators produce more nonchaotic behavior than the uncoupled system was not expected. Is this an artifact of the numerical methods used or is this truly how this system behaves? If it is truly how the system behaves, why does this happen? Is there a global attractor to which all initial conditions are drawn?

We also observed an interesting phenomena when looking at the coupled clocks. As we varied the damping there was a transition from in-phase synchronization to out-of-phase synchronization. This suggests that there is a bifurcation which occurs at the critical damping. It would be interesting to study the dynamics behind this bifurcation.

Another area where more work can be done is in visualizing the data. Both coupled oscillators live in a six dimensional phase space. To see our data we looked at two dimensional graphs. We could look at three dimensional plots, which could potentially yield more information. Additionally, we could also look at other ways to analyze the data. We primarily looked at graphs which seemed to indicated certain phenomena, but a more formal analysis would be needed to show these actually exist (and are not simply an artifact of the numerical methods).

We focused on the changes in the dynamics as we varied the damping in the coupled clocks. For the coupled driven pendulums we varied damping, forcing, and drive frequency. What happens to the dynamics as we vary the ratio of the mass of the beam to the mass of the pendulum? This would be an interesting question for both systems. It would also be interesting to fix the system parameters and simply vary the initial conditions. Both of these could be compared to experimental results for the coupled clocks.

While the work done here has shown some interesting results, there is still much left to explore. Perhaps another off-the-wall observation will be made while lying in bed and spark a whole new realm of discovery.

Supplemental Website

One of the limitations in presenting this material in a written paper is fitting the graphs on a sheet of paper. For example, in Figure 4.2 we look at 500 seconds worth of a time series. I presented the first 50 seconds and last 25 second to show how the system started and ended. However if I placed all 500 seconds on a sheet of paper it would be hard to discern what is happening. To present the reader with the whole picture I have placed larger images on-line which one can scroll through to see the entire time series. I have also placed higher resolution pictures of other plots, such as the Poincaré section of the driven pendulum in Figure 3.6b.

The website can be found at `http://thesis.lebailly.us/`.

Bibliography

[1] V. I. Arnol′d. *Mathematical methods of classical mechanics*, volume 60 of *Graduate Texts in Mathematics*. Springer-Verlag, New York, second edition, 1989. Translated from the Russian by K. Vogtmann and A. Weinstein.

[2] Karl Johan Åström and Richard M. Murray. *Feedback systems*. Princeton University Press, Princeton, NJ, 2008. An introduction for scientists and engineers.

[3] Gregory L. Baker and James A. Blackburn. *The pendulum*. Oxford University Press, Oxford, 2005. A case study in physics.

[4] K. Czolczynski, P. Perlikowski, A. Stefanski, and T. Kapitaniak. Huygens' odd sympathy experiment revisited. *International Journal of Bifurcation and Chaos*, 21(07):2047–2056, 2011.

[5] Vojin Jovanovic and Sergiy Koshkin. Synchronization of huygens' clocks and the poincaré method. *Journal of Sound and Vibration*, 331(12):2887 – 2900, 2012.

[6] William H. Press, Saul A. Teukolsky, William T. Vetterling, and Brian P. Flannery. *Numerical recipes in C*. Cambridge University Press, Cambridge, second edition, 1992. The art of scientific computing.